THE AMERICAN SOCIETY OF MECHANICAL ENGINEERS
345 E. 47th St., New York, N.Y. 10017

96-GT-69

SIMULATION OF 3D-UNSTEADY STATOR/ROTOR INTERACTION IN TURBOMACHINERY STAGES OF ARBITRARY PITCH RATIO

Alexander R. Jung, Jürgen F. Mayer and Heinz Stetter
Institut für Thermische Strömungsmaschinen und Maschinenlaboratorium
University of Stuttgart
Stuttgart, Germany

ABSTRACT

This paper presents a computational method for the calculation of unsteady three-dimensional viscous flow in turbomachinery stages. The method is based on a Finite-Volume Navier-Stokes solver for structured grids in a multiblock topology. The meshes at the stator/rotor interface are overlapped by two grid cells. An implicit residual smoothing method applicable to global time-stepping is used to accelerate the solution process.

The problem of periodic boundary treatment for unequal pitches is handled using a method of time-inclined computational domains for three dimensions. The method applies a time transformation to the stator domain and to the rotor domain and uses different time-steps in the two domains.

The results of a numerical simulation of the flow in a transonic turbine stage with a pitch ratio of 1.364 are presented. The time-averaged solution is compared to experimental data and satisfactory agreement is stated. Complex 3D-unsteady flow phenomena (shock motion, vortex shedding) are observed. Unsteady blade pressure fluctuations at various positions in spanwise direction are shown and the fluctuations are found to vary considerably along span. Instantaneous distributions of static pressure, Mach number, and entropy are presented.

INTRODUCTION

During the last years several papers were published describing numerical methods for the calculation of the three-dimensional unsteady viscous flow in turbomachinery. The 3D-Navier-Stokes solvers described by Rai and Madavan (1990) and Dawes (1994) use a ratio of small integers as an approximation to the pitch ratio and perform simulations with multiple blade passages. In order to maintain the pitch-chord ratio the blades of the downstream cascade are scaled in these methods. Arnone and Pacciani (1995) perform a 2D-Navier-Stokes analysis of a turbine stage using different integer approximations up to the exact pitch ratio. They state significant differences in the rotor lift evolution as well as in the frequency spectra especially if the adjustment in the blade pitches is greater than 1%. In an early approach Erdos et al. (1977) proposed to store the solutions at the pitchwise boundaries at every time step during a blade passing period and to use them as boundary conditions for the subsequent period, what implies, that the flow is periodic in time. Using solutions of the previous period, however, leads to slow convergence to a periodic solution and may completely fail to converge in cases of viscous flow if there exist other frequencies besides the blade passing frequency (e.g. self excited trailing edge vortex shedding). Giles (1990) showed with his 2D-Euler simulations of complex shock motion in the axial gap between the stator and the downstream rotor the importance of using the exact pitch ratio in the numerical simulation. He developed a method to handle the problem of periodic boundary treatment for any pitch ratio hy performing time transformations and using different time steps for the stator and rotor domains.

The numerical method described in this paper allows 3D-unsteady viscnus flow analysis in turbomachinery stages of arbitrary pitch ratio and uses Giles' method for the periodic boundary treatment. It is based on a Navier-Stokes solver developed at the Institut für Thermische Strömungsmaschinen und Maschinenlaboratorium (ITSM) of the University of Stuttgart (Merz et al., 1995), which has been extended to unsteady flow simulations (Jung et al., 1995).

GOVERNING EQUATIONS

The equations solved are the nondimensionalized, Favre-averaged Navier–Stokes equations written for a cylindrical coordinate system rotating with constant angular velocity Ω around the x-axis:

$$\int_V \frac{\partial \vec{Q}}{\partial t} dV + \int_A \left(\vec{F}_x r d\varphi dr + \vec{F}_\varphi dx dr + \vec{F}_r r dx d\varphi \right) + \int_V \vec{S} dV = 0 \quad (1)$$

$$\vec{Q} = \left[\varrho, \quad \varrho w_x, \quad \varrho w_\varphi, \quad \varrho w_r, \quad \varrho e_t \right]^T \quad (2)$$

Presented at the International Gas Turbine and Aeroengine Congress & Exhibition
Birmingham, UK — June 10-13, 1996

$$\vec{F}_x = \begin{bmatrix} \varrho w_x \\ \varrho w_x^2 + p + \tau_{xx} \\ \varrho w_\varphi w_x + \tau_{\varphi x} \\ \varrho w_r w_x + \tau_{rx} \\ (\varrho e_t + p) w_x + q_x \end{bmatrix} \quad \vec{F}_\varphi = \begin{bmatrix} \varrho w_\varphi \\ \varrho w_x w_\varphi + \tau_{x\varphi} \\ \varrho w_\varphi^2 + p + \tau_{\varphi\varphi} \\ \varrho w_r w_\varphi + \tau_{r\varphi} \\ (\varrho e_t + p) w_\varphi + q_\varphi \end{bmatrix} \tag{3}$$

$$\vec{F}_r = \begin{bmatrix} \varrho w_r \\ \varrho w_x w_r + \tau_{xr} \\ \varrho w_\varphi w_r + \tau_{\varphi r} \\ \varrho w_r^2 + p + \tau_{rr} \\ (\varrho e_t + p) w_r + q_r \end{bmatrix} \quad \vec{S} = \frac{1}{r} \begin{bmatrix} 0 \\ 0 \\ \varrho w_r (w_\varphi + 2\Omega r) + \tau_{r\varphi} \\ -\varrho (w_\varphi + \Omega r)^2 - p - \tau_{\varphi\varphi} \\ 0 \end{bmatrix} \tag{4}$$

where ϱ, w_x, w_φ, w_r, and e_t denote density, relative velocity components in the x, φ, and r directions, and relative specific total energy, respectively. The shear–stress tensor and the vector of shear-stress-energy-transfer and heat-transfer for a Newtonian fluid are calculated as follows:

$$\bar{\bar{\tau}} = -\mu \begin{bmatrix} 2\frac{\partial w_x}{\partial x} + \Lambda & \frac{1}{r}\frac{\partial w_x}{\partial \varphi} + \frac{\partial w_\varphi}{\partial x} & \frac{\partial w_x}{\partial r} + \frac{\partial w_r}{\partial x} \\ \vdots & 2\left(\frac{1}{r}\frac{\partial w_\varphi}{\partial \varphi} + \frac{w_r}{r}\right) + \Lambda & \frac{\partial w_\varphi}{\partial r} - \frac{w_\varphi}{r} + \frac{1}{r}\frac{\partial w_r}{\partial \varphi} \\ \text{sym.} & \cdots & 2\frac{\partial w_r}{\partial r} + \Lambda \end{bmatrix}$$

$$\Lambda = \frac{\lambda}{\mu}\left(\frac{\partial w_x}{\partial x} + \frac{1}{r}\frac{\partial w_\varphi}{\partial \varphi} + \frac{w_r}{r} + \frac{\partial w_r}{\partial r}\right) \tag{5}$$

$$\vec{q} = \begin{bmatrix} \tau_{xx} w_x + \tau_{x\varphi} w_\varphi + \tau_{xr} w_r - k\frac{\partial T}{\partial x} \\ \tau_{\varphi x} w_x + \tau_{\varphi\varphi} w_\varphi + \tau_{\varphi r} w_r - k\frac{1}{r}\frac{\partial T}{\partial \varphi} \\ \tau_{rx} w_x + \tau_{r\varphi} w_\varphi + \tau_{rr} w_r - k\frac{\partial T}{\partial r} \end{bmatrix} \tag{6}$$

The relations between the nondimensional variables are given by the caloric and thermal state equations for an ideal gas with constant ratio κ of specific heat capacities,

$$p = (\kappa - 1)\left(\varrho e_t - \frac{\varrho}{2}\left(w_x^2 + w_\varphi^2 + w_r^2 - \Omega^2 r^2\right)\right) \quad , \quad T = \frac{p}{\varrho} \quad . \tag{7}$$

The effect of turbulence is taken into account using the eddy–viscosity hypothesis. The nondimensional viscosity μ in Eq. (5) and the thermal conductivity k in Eq. (6) are set to

$$\mu = \mu_l + \mu_t \quad \text{and} \quad k = \frac{\kappa}{\kappa - 1}\left(\frac{\mu_l}{Pr_l} + \frac{\mu_t}{Pr_t}\right) \quad , \tag{8}$$

where Pr_l and Pr_t denote the laminar and turbulent Prandtl numbers, respectively. The laminar viscosity μ_l is assumed to follow the empirical power law

$$\mu_l(T) = \mu_l(T_0)\left(\frac{T}{T_0}\right)^{0.75} \quad . \tag{9}$$

Here $\mu_l(T_0)$ is assumed constant for a given reference temperature T_0. According to Stokes hypothesis, tbe parameter for lateral contraction λ is set to $-2\mu_l/3$. The turhulent viscosity μ_t and the turbulent Prandtl number Pr_t are determined using a modified Baldwin and Lomax (1978) turbulence model. The contributions to the eddy viscosity are computed separately for the blade–to–blade direction η and the spanwise direction ζ. The squares of the wall distances d_η and d_ζ are used to compute the resulting eddy viscosity

$$\mu_t = f\,\mu_{t\,\eta} + (1 - f)\,\mu_{t\,\zeta} \quad , \quad \text{where} \quad f = \frac{d_\zeta^2}{d_\eta^2 + d_\zeta^2} \quad . \tag{10}$$

The shear layers on the end walls are assumed fully turbulent from the inlet boundary while the transitional criterion of Baldwin and Lomax is used on the blade surface.

DISCRETIZATION

The system of five equations (1) is discretized in space in Finite-Volume form on each curved hexahedral cell of a structured mesh to yield

$$\frac{\partial}{\partial t}\vec{Q}_{i,j,k} = -\frac{1}{V_{i,j,k}}\left(\vec{R}_c + \vec{R}_d + \vec{D}\right)_{i,j,k} \quad , \tag{11}$$

where $V_{i,j,k}$ denotes the volume of the control hexahedron for each point $P_{i,j,k}$. The vectors $\vec{R}_c$ and $\vec{R}_d$ account for the convective and the diffusive terms, respectively, including the corresponding source terms. $\vec{D}$ denotes the artifical dissipation. The solutions are located at the vertices of the hexahedrons.

The residual $\vec{R}_c$ of the convective terms is calculated at each point $P_{i,j,k}$ of the computational domain by adding the contributions of the eight cells which have this point in common. Following a method based on the work of Radespiel et al. (1989), an auxiliary hexahedron with its edges located in the centers of the eight cells of the control volume is used to compute the residual of the diffusive terms $\vec{R}_d$.

Artificial dissipation $\vec{D}$ is added to the discretized equations using an extension of the model introduced by Jameson et al. (1981) to prevent odd-even point decoupling and oscillations near shock waves. In order to minimize the artificial dissipation in the boundary layer, variable scaling factors are used to account for the spectral radii and for the variations of the cell's aspect ratios, see Radespiel et al. (1989).

The system of ordinary differential equations (11) is discretized in time using an explicit five-stage Jameson-type Runge-Kutta time-stepping scheme. Global time steps are used to ensure a time accurate calculation.

The artificial dissipatinn terms are calculated for stage 1, 3 and 5, respectively. For cnmputational efficiency, the diffusive terms are evaluated only for stage 1 of the scheme and assumed constant for stages 2 to 5, see Merz et al. (1995).

IMPLICIT RESIDUAL SMOOTHING

Due to the global time stepping, the maximum allowable time step of the basic scheme is limited by the stability limit of the finest grid cells which are nsually in the boundary layers on solid surfaces or in the very fine viscous grid regions around the blades' leading and trailing edges, whereas in the more inviscid main portion of the computational domain larger grid cells would allow for a much larger time step (typically 50 to 100 times larger than in the viscous regions). Under the assumption that in the viscous regions an increase of the time step by a factor of 10 still gives reasonable time-accuracy, computational efficiency can be increased by the same factor.

The idea here is to use an implicit operator to stabilize the explict time integration only at those points where the stability condition is violated because of the increased time step. All other points that are well within the stability limit do not need special attention.

The implicit smoothing algorithm for unsteady calculations described below is based on the method proposed hy Jorgenson and Chima (1989) but uses directionally-influenced smoothing in order to minimize the smoothing in those coordinate directions that do not determine the stability.

If the residual $\Delta\vec{Q}^{(k)}$ at stage k of the Runge-Kutta scheme with the coefficients α_k is written as

$$\Delta\vec{Q}^{(k)} = -\alpha_k \frac{\Delta t}{V}\left(\vec{R}_c + \vec{R}_d + \vec{D}\right) \quad , \tag{12}$$

then the implicit smoothing operator is given by

$$(1-\varepsilon_\xi\delta_{\xi\xi})(1-\varepsilon_\eta\delta_{\eta\eta})(1-\varepsilon_\zeta\delta_{\zeta\zeta})\overline{\Delta\vec{Q}^{(k)}} = \Delta\vec{Q}^{(k)}$$
$$\vec{Q}^{(k)} = \vec{Q}^{(0)} + \overline{\Delta\vec{Q}^{(k)}} \quad , \tag{13}$$

where $\overline{\Delta\vec{Q}^{(k)}}$ is the smoothed residual, $\delta_{\xi\xi}$, $\delta_{\eta\eta}$, and $\delta_{\zeta\zeta}$ denote the second-difference operators, and ε_ξ, ε_η and ε_ζ are the smoothing parameters in a curvilinear coordinate system with the ξ, η, and ζ coordinates following the grid lines in axial, circumferential, and radial direction, respectively.

For sufficiently large values of ε_ξ, ε_η, and ε_ζ the Runge-Kutta scheme can be made unconditionally stable without affecting the second order accuracy in space, provided the smoothing parameters are not too large. Also, as Jorgenson and Chima (1989) show, the smoothing has no effect on the temporal accuracy of the unsteady scheme since it is done in space rather than in time.

In unsteady calculations, the local Courant number varies substantially over the grid since the time step is spatially constant. In order to smooth only those regions where the local Courant number CFL^{loc} is larger than the maximum Courant number CFL^* of the time stepping scheme, the smoothing parameters are calculated using

$$\varepsilon_i = \max\left\{0, \frac{1}{4}\left[\left(\frac{CFL_i^{loc}}{CFL^*}\right)^2 - 1\right]\right\} \quad , \quad i \in \{\xi,\eta,\zeta\} \quad , \tag{14}$$

where

$$\frac{CFL_i^{loc}}{CFL^*} = \frac{CFL}{CFL^*}\frac{\Delta t_{min}}{\Delta t_i^{loc}} \quad . \tag{15}$$

Here CFL denotes the Courant number to use for the cell which determines the global time step Δt_{min}. Δt_i^{loc}, $i \in \{\xi,\eta,\zeta\}$ is the local time step limit in the corresponding direction. The time steps in discussion satisfy

$$\Delta t_{min} = \left(\frac{1}{\min\{\Delta t_\xi^{loc}, \Delta t_\eta^{loc}, \Delta t_\zeta^{loc}\}} + \frac{1}{\Delta t_d}\right)^{-1} \quad , \tag{16}$$

$$\Delta t_\xi^{loc} = V\left(\max\left\{(\lambda_\xi+\lambda_\eta+\lambda_\zeta)_{i\pm\frac{1}{2},j,k}\right\}\right)^{-1} \quad ,$$

$$\Delta t_\eta^{loc} = V\left(\max\left\{(\lambda_\xi+\lambda_\eta+\lambda_\zeta)_{i,j\pm\frac{1}{2},k}\right\}\right)^{-1} \quad , \tag{17}$$

$$\Delta t_\zeta^{loc} = V\left(\max\left\{(\lambda_\xi+\lambda_\eta+\lambda_\zeta)_{i,j,k\pm\frac{1}{2}}\right\}\right)^{-1} \quad ,$$

$$\Delta t_d = V^2\left(2\vec{A}^2\frac{\mu_l+\mu_t}{\varrho}\max\left\{\frac{4}{3}, \frac{\gamma}{Pr}\right\}\right)^{-1} \quad , \tag{18}$$

where λ_i, $i \in \{\xi,\eta,\zeta\}$ are the contravariant eigenvalues of the linearized Euler Equations and $\vec{A}^2$ is the sum of the squares of the auxiliary cell's surface vectors. The global time step Δt which is used in the solution progress (12) is then given by

$$\Delta t = CFL\,\Delta t_{min} \quad . \tag{19}$$

Note that in Eqs. (16) to (19) Δt_{min} is the only globally determined time step. The other time steps are based on the individual grid cells and thus are computed locally.

The smoothing procedure is applied during each of the five Runge-Kutta stages. In order to get the maximum smoothing effect, all neighbouring grid blocks of the multiblock grid are taken into account as if the domain consisted of only a single block. At the stator/rotor interface, the residuals of the two domains are interchanged in a way similar to coupling the flow variables. This has the advantage that the residuals of the overlapping grid cells can then be added to the smoothing procedure to improve smoothing in this area.

BOUNDARY CONDITIONS

Non-reflecting boundary conditions are used at the inlet and outlet boundaries to keep computational domains small without introducing spurious reflections from outward travelling waves. The method, Merz et al. (1995), is an extension of the work of Giles (1988) and Saxer (1992) to viscous flow boundary conditions and meshes with non-equidistant spacing.

Solid walls are assumed adiabatic and the no-slip condition $\vec{w} = \vec{0}$ is applied to the updated velocity components after each stage of the Runge-Kutta scheme. Since this results in a decrease in kinetic energy, the density and relative total energy are corrected in the course of which entropy and relative total enthalpy are conserved.

Periodicity in the pitchwise direction is ensured through the use of phantom cells that keep copies of the periodic values. In this way, the points at the periodic boundaries can be treated like interior points and do not need special treatment.

ARBITRARY STAGE PITCH RATIO

In calculations of unsteady flow in turbomachinery stages where the number of stator blades is different from the number of rotor blades a problem arises which is not present in steady state calculations: The number of pitchwise periodic boundaries in a stator/rotor configuration is equal to the largest common divisor of the number of rotor blades and the number of stator blades. In the worst but not unrealistic case where the common divisor is equal to one, this means that all blade passages of the stator and the rotor would have to be used in the simulation since integration of the system of equations (11) cannot be carried out without a full set of boundary conditions. Even with today's supercomputers it is difficult to get a reasonable unsteady Navier-Stokes simulation that includes all blade passages of a turbomachinery stage. Therefore, a method is neccessary that allows to apply simple periodicity conditions on small computational domains independently of the stage's pitch ratio and without modifying or scaling geometry.

These claims lead to the idea of using time-inclined computational domains: Use a reversible transformation to transform the whole flow problem from the physical (x,φ,r,t) space into a computational (x',φ',r',t') space in which pitchwise boundaries are periodic boundaries even if they are not periodic in the physical space. The method described here is based on the work of Giles (1991) and has been extended to three-dimensional viscous flow on non-equidistant meshes, Jung et al. (1995).

If the transformation is defined as

$$\begin{aligned} x' &= x \,, \\ \varphi' &= \varphi \,, \\ r' &= r \,, \\ t' &= t - \lambda\varphi \,, \\ \lambda &= \begin{cases} \frac{\Delta T}{\varphi_S} & \text{for the stator domain} \\ \frac{\Delta T}{\varphi_R} & \text{for the rotor domain} \end{cases} , \end{aligned} \tag{20}$$

then the vector of conserved quantities changes from $\vec{Q}$ to $\vec{Q}'$, where

$$\vec{Q}' = \vec{Q} - \lambda\vec{F}_\varphi \quad . \tag{21}$$

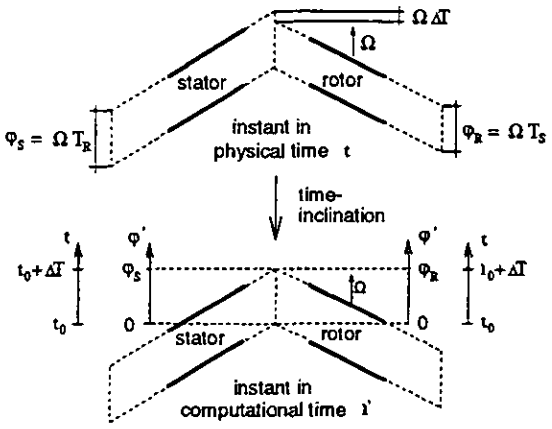

Figure 1: Effect of the time-inclination on turbomachinery stages with different pitches of stator and rotor

The overall structure of the sytem of equations to be solved (1) is not affected by this transformation. In Eq. (20) φ_S and φ_R denote the stator pitch and the rotor pitch, respectively. The fundamental quantity of the transformation is the time lag

$$\Delta T = T_R - T_S = (\varphi_S - \varphi_R)/\Omega \quad . \tag{22}$$

It represents the difference between the rotor blade passing period T_R and the stator blade passing period T_S. It can be viewed as the amount of time, which the upper pitchwise boundary lags the lower pitchwise boundary to be periodic, since in physical space the periodicity condition is

$$\vec{Q}(\varphi, t) = \vec{Q}(\varphi + \varphi_i, t + \Delta T) \quad , \quad i \in (S, R) \quad , \tag{23}$$

for points in the stator domain (index S) and in the rotor domain (index R), respectively. Applying the transformation equations yields the wanted result: at any specific instant in computational time t' the difference in physical time between the corresponding points at the upper and lower pitchwise boundaries of the stator as well as rotor domain amounts to the time lag ΔT, see Fig. 1. Therefore simple periodicity conditions may be applied,

$$\vec{Q}'(\varphi', t') = \vec{Q}'(\varphi' + \varphi_i, t') \quad , \quad i \in (S, R) \quad . \tag{24}$$

Note that, as opposed to the approaches mentioned in the introduction, the method presented here requires neither any assumption concerning the flow at the pitchwise boundaries nor any geometry adjustment. Therefore it is able to reproduce all frequencies that are present in the flow field.

For inviscid flow with ideal gas, the flow variables $\vec{Q}$ can be computed analytically from $\vec{Q}'$. For viscous flow this equation describes a differential algebraic system of equations. In a first approach the differentials in Eq. (21) are simply ignored. The neglected terms are comparable in magnitude to those that are usually dropped in the thin-shear-layer Navier-Stokes equations under high Reynolds number conditions, Giles (1991).

The calculation of $\vec{Q}$ from $\vec{Q}'$ then leads to a quadratic equation for the static pressure. The investigation of its solutions yields the condition (Giles (1991), Jung et al. (1995))

$$(1 - \gamma w_\varphi)^2 - \gamma^2 a^2 \geq 0 \quad , \quad a = \sqrt{\kappa p/\varrho} \quad , \quad \gamma = \lambda/r \quad , \tag{25}$$

which is only true provided that

$$-\frac{1}{a - w_\varphi} \leq \gamma \leq \frac{1}{a + w_\varphi} \quad . \tag{26}$$

This means that the inclination parameter λ is limited by the physical characteristics of the linearized Euler equations. This is a reasonable and fundamental limitation as without this constraint information which is propagating forward in physical time could be propagating backward in the computational time. This violates the principle of causality and is inconsistent with an integration algorithm that marches forward in time. Therefore stator/rotor configurations with big differences in the pitches cannot be simulated using only one stator channel and one rotor channel. With the use of multiple blade passages the inclination parameter can be reduced to a value that allows a stable simulation. It should be noted that the memory requirement for the calculation does not increase linearly with the number of blade passages used since neighbouring flow channels have identical geometries.

At the end of the computation, the solutions at different instants of the computational time are transformed back to obtain solutions at different instants of the physical time. This is done by storing the solutions at a number of time-steps (typically 40–100) during the last blade passing period of the computation. After the simulation the desired number of solutions at the desired instants of the physical time are calculated from the stored solutions.

STATOR/ROTOR INTERFACE

The meshes at the stator/rotor interface are overlapped by two grid cells in axial direction (phantom cells). The direct interaction of the flows in the two domains is realized by coupling the residuals and the smoothing parameters during each Runge-Kutta stage as well as by coupling the flow variables after each stage. For that purpose a four step algorithm is used:

1. The quantities at the points of the phantom cells of the upstream domain are interpolated from the values at the corresponding points of the downstream domain, Fig. 2.
2. Same as 1. but for the phantom cells of the downstream domain.
3. The quantities at the points of the upstream plane of the sliding interface are averaged with those of the downstream plane of the sliding interface.
4. Same as 3. but for the downstream plane of the sliding interface.

It should be noted that in order to couple the quantities of the two domains, they have to be described in the same frame of reference. Therefore the quantities of the interface region are transformed into one frame before they are interchanged and are transformed back after coupling is done. Also, dependent on which quantity is being interchanged, different transformation equations apply, Jung et al. (1995).

RESULTS

The simulation was carried out for the last stage of a low pressure turbine operated at ITSM. The stage has 44 stator blades and 60 rotor blades giving a pitch ratio of 1.364. The rotational speed is 12,600 rpm. Due to the long and strongly twisted blades the Mach numbers associated with the rotor speed varies from about 0.6 at the hub to about 1.4 at the casing. These operating conditions lead to high relative velocities in circumferential direction w_φ such that the stability condition

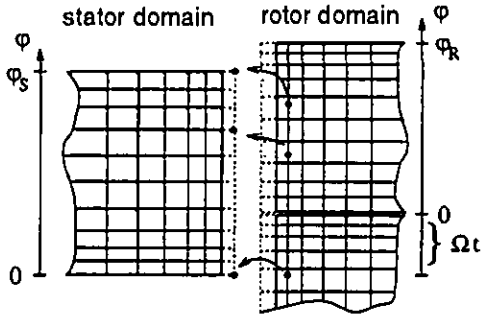

Figure 2: Coupling of stator grid with rotor grid (step 1)

(26) is violated when using only a single stator blade passage and a single rotor blade passage. The use of one stator passage and two rotor passages would lead to an even higher pitch ratio ($44/30 = 1.4667$). Using a configuration consisting of two stator passages and three rotor passages reduces the pitch ratio to $22/20 = 1.1$ and a stable calculation can be performed.

The computational grid on the blade surfaces and on the hub is shown in Fig. 3. Each of the stator channels is discretized with $53 \times 31 \times 51$ grid points in axial, circumferential, and radial direction, respectively. One rotor channel consists of $57 \times 31 \times 51$ grid points. This makes up a total of 437,937 nodes for the whole computational domain. In preparation of the calculation shown in this paper, several computations with different smoothing coefficients were carried out. It was found that for this quite coarse mesh a gain in computational efficiency of a factor between 5 and 6 compared to a calculation without residual smoothing can be achieved without noticeable changes in the boundary layer behaviour. The calculation required 84 MBytes of memory and was performed on a 175 MHz DEC-Alpha desktop workstation. Each time step took about 216 seconds of CPU time. Starting from a steady state solution, ten stator domain passing periods (corresponding to 30 rotor channels passing a stator channel) were calculated to minimize transient disturbances. Each domain passing period took about 330 time steps.

During the last period 100 solutions were stored requiring temporarily 865 MBytes of disk space. After the simulation, flow fields at 50 different instants of physical time during one stator blade passing period were calculated from the stored solutions. The time averaged flow variables $\bar{q}$ and the standard deviation (rms-fluctuation) $\tilde{q}$ were determined according to

$$\bar{q} = \frac{1}{N}\sum_{n=1}^{N} q(n) \quad , \quad \tilde{q} = \sqrt{\frac{1}{N-1}\sum_{n=1}^{N}(q(n)-\bar{q})^2} \quad , \qquad (27)$$

where N is the number of stored solutions. The pressure fluctuations were normalized by the time-mean pressure.

Figure 4 shows experimental data (Zimmermann, 1994) in comparison to circumferentially averaged values of the time averaged numerical solution for the stator inlet (top row), the stator/rotor interface (middle row) and the rotor exit (bottom row). The experimental values of the total pressure and the flow angle at the stator inlet and the static pressure at the rotor exit are used as part of the boundary conditions and thus are identical to the numerical values. The agreement of the other quantities at the stator inlet and the stator/rotor

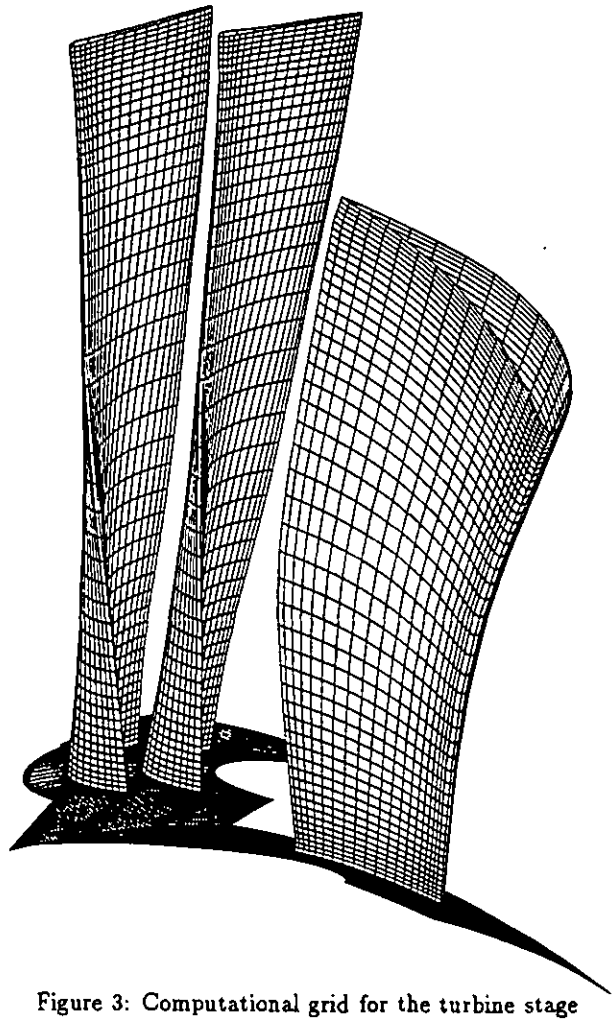

Figure 3: Computational grid for the turbine stage

interface is very similar to that of the results of a steady state calculation (Merz et al., 1995) although there is a high level of unsteadiness in the axial gap between the stator and the rotor. This similarity can be explained by the fact that the flow is transonic in the region of high unsteady fluctuation such that information is propagating mainly downstream. Therefore there is only little interaction of the flow with solid walls which would lead to big changes in the time-mean flow field upstream of the rotor blade leading edge. The development of the various flow phenomena in the rotor (e.g. passage vortex or vortex shedding from the trailing edge), however, depends strongly on the rotor inlet flow conditions, so that at the rotor exit (Fig. 4, bottom row) the overall agreement of the time-averaged unsteady results and the experimental data is better than that of the steady state calculation and the experiments. Especially the prediction of the flow angle near the hub region is closer (about 8°) to the experimental values. The influence of the passage vortex on the exit flow angle can be clearly seen in the diagram. The core of the vortex lies in the region between 10 % and 20 % span as can be seen e.g. in Fig. 11 but there are no experimental data for this region. The effect of obtaining a more accurate prediction of the exit flow angle by performing an unsteady rather than a steady state calculation was also shown by Gallus et al. (1994).

The diagrams in Fig. 6 show normalized rms-fluctuations of the unsteady static pressure distributions on the rotor blades at twelve different spanwise positions. Due to the long and strongly twisted blades, the character of the flow varies considerably along span. Up to 31 % span the fluctuations increase to a maximum at about 30 % axial chord on the suction side that amounts to almost 23 % of the time-mean value. The maximum of the fluctuations on the pressure side is also at 31 % span and amounts to almost 19 % of the time mean value. But unlike for the suction side the maximum is found near the trailing edge at about 90 % axial chord. These strong fluctuations are due to shock waves that emerge from the stator blades' trailing edges in those regions where the stator outflow is transonic and interact with the rotor blades. Due to the quite coarse discretization, the shocks are not very sharp but they can be seen in the contour plots of instantaneous static pressure (Fig. 9a) and absolute Mach number (Fig. 9b). Complex pressure wave motion can be seen from the pressure contours as each of the flow channels can be viewed as the same channel at different instants of time. Here should he noted that the unsteady coupling procedure is flux conserving across the interface and that the slight disturbances of the pressure and Mach number contours are completely in the rotor domain. The cause for these wiggles is currently being investigated. We suspect it to be an insufficiency in turbulence modelling. The region where the stator outflow is transonic ends at about 60 % span. Additionally the relative blockage of the flow by the rotor blades decreases as the blades become thinner and as the flow channel becomes wider with increasing radius. As a consequence, the unsteady fluctuations decrease in spanwise direction and remain below 5 % above 60 % span. Please note in Fig. 6 the different ordinate scalings for this region.

The contour plots in Fig. 7 show the radial distributions of the unsteady fluctuations of static pressure $\tilde{p}_{stat}$, relative Mach number $\tilde{Ma}_{rel}$ and entropy $\tilde{\Delta s}$ in the blade-to-blade channel of the rotor at about 30 % and 80 % chord length, respectively. The region of high unsteadiness with the maximum at about 30 % span can be clearly seen.

Figures 5 and 8 show unsteady blade pressure distributions at 31 % span at different instants of time during a rotor blade passing period. The pressure is nondimensionalized by the maximum total pressure at the stator inlet (275 mbar). The motion of the pressure wave on the suction side is almost sinusoidal with the clearly visible maximum at about 30 % axial chord whereas the motion of the pressure wave on the pressure side is more complicated due to waves that are reflected from the neighbouring blade suction side. For better comparison, in Fig. 8 the time averaged pressure distributions are plotted together with the unsteady pressures.

Instantaneous relative Mach number contours in a cross-flow section at about 75 % of the axial gap between the stator and the rotor are shown in Fig. 10. Near the casing potential flow effects of the rotor blades are visible, whereas in the region of 50 % span and below the influence of the wakes from the 4.4 stator passages that face the 6 rotor passages are dominant.

Figure 11 shows unsteady entropy contours in a cross-flow section near the exit of the rotor domain. In the lower 50 % span several stages of vortices shed from the rotor blade trailing edges and leaving the domain can be seen. An azimuthal cut which shows this phanomenon more clearly is shown in Fig. 9c.

CONCLUSIONS

A numerical method for the calculation of unsteady stator/rotor interaction in turbomachinery stages of arbitrary pitch ratio is presented. Results of a simulation of the unsteady flow in the last stage of a highly loaded transonic turbine are shown. Comparison with experimental data is made and satisfactory agreement is stated. Especially, the prediction of the rotor exit flow angle is closer to the experimental values than in a steady state calculation. Unsteady results are shown. A complex three-dimensional flow field that varies significantly along the span can be found. Shock waves emerging from the stator blade trailing edges interact with the rotor flow field. The change of unsteady lift on the rotor blades causes vortices to be shed from the rotor blade trailing edges. Further investigations on finer grids of this and other turbomachinery stages under inclusion of overtip leakage flows need to be done to quantify and better extract the existing flow phenomena.

REFERENCES

Arnone, A., Pacciani, R., 1995, "Rotor-Stator Interaction Analysis Using the Navier-Stokes Equations and a Multigrid Method," ASME 95-GT-177.

Baldwin, B. S., Lomax, H., 1978, "Thin Layer Approx. and Algebraic Model for Separated Turbulent Flows," AIAA 78-257.

Dawes, W. N., 1994, "A Numerical Study of the Interaction of a Transonic Compressor Rotor Overtip Leakage Vortex with the Following Stator Blade Row," ASME 94-GT-156.

Erdos, J. I., Alzner, E., McNally, W., 1977, "Numerical solution of periodic transonic flow through a fan stage," AIAA Journal, vol. 15, no. 11, pp. 1559–1568.

Gallus, H. E., Zeschky, J., Hah, C., 1994,"Endwall and Unsteady Phenomena in an Axial Turbine Stage," ASME 94-GT-143.

Giles, M. B., 1988, "Non-Reflecting Boundary Conditions for the Euler Equations," Tech. Rep. TR-88-1, MIT Computational Fluid Dynamics Laboratory.

Giles, M. B., 1990, "Stator/Rotor Interaction in a Transonic Turbine," *AIAA J. Prop. Power*, vol. 6(5), pp. 621–627.

Giles, M. B., 1991, "UNSFLO: A Numerical Metbod for the Calculation of Unsteady Flow in Turbomachinery," GTL Rep. No. 205, MIT Gas Turbine Laboratory.

Jameson, A., Schmidt, W., Turkel, E., 1981, "Numerical Solutions of the Euler Equations by Finite Volume Methods Using Runge Kutta Time-Stepping Schemes," AIAA 81-1259.

Jorgenson, P., Chima, R., 1989, "An Unconditionally Stable Runge-Kutta Method for Unsteady Flows," AIAA 89-0205.

Jung, A., Stetter, H., 1995, "Berechnung der Stator-Rotor-Interaktion in Turbomaschinen," DFG-Bericht Ste 489/8-1.

Merz, R., Krückels, J., Mayer, J. F., Stetter, H., 1995, "Computation of Three–Dimensional Viscous Transonic Turbine Stage Flow Including Tip Clearance Effects," ASME 95–GT–76.

Radespiel, R., Rossow, C.-C., Swanson, R. C., 1989, "An Efficient Cell–Vertex Multigrid Scheme for the Three–Dimensional Navier–Stokes Equations," AIAA 89–1953.

Rai, M. M., Madavan, N. K., 1990, "Multi-Airfoil Navier–Stokes Simulations of Turbine Rotor-Stator Interaction," *J. Turbomach.*, vol. 112, pp. 377–384.

Saxer, A. P., 1992, "A Numerical Analysis of 3-D Inviscid Stator/Rotor Interactions Using Non-Reflecting Boundary Conditions," PhD Th., Gas Turb. Lab., MIT, Cambridge, MA.

Zimmermann, C., 1994, "Experimentelle Bestimmung des Strömungsfeldes einer ND–Modellturbine im Bereich der Endstufe und des anschließenden axiradialen Diffusors," Dissertation, University of Stuttgart.

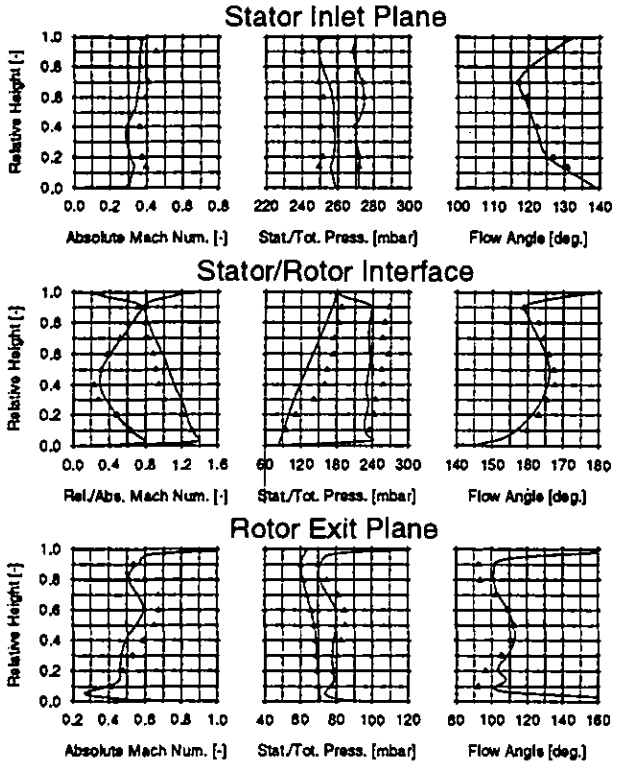

Figure 4: Comparison of experimental data (symbols) with circumferentially and time averaged numerical data (solid lines)

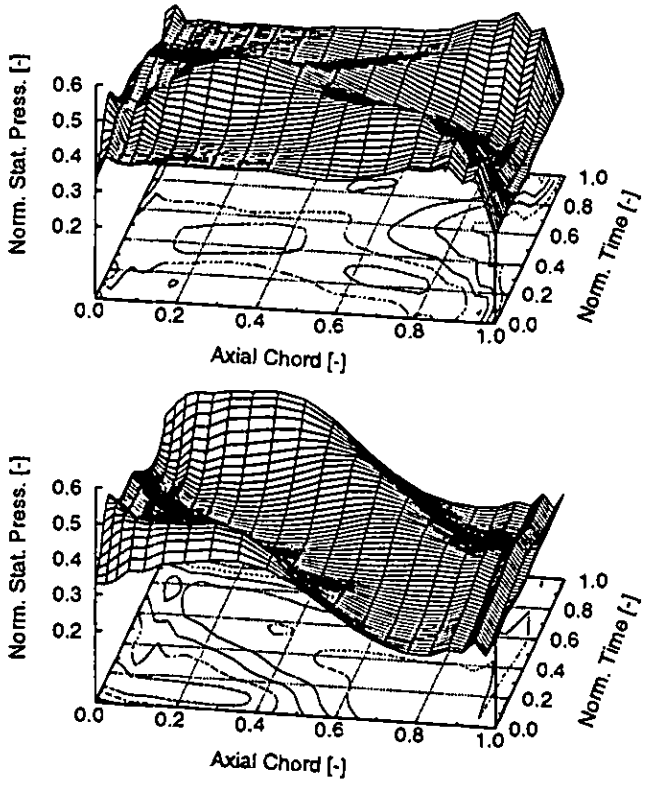

Figure 5: Unsteady Pressure distributions on the pressure side (top) and on the suction side (bottom) of the rotor blade at 31 % span during one rotor blade passing period

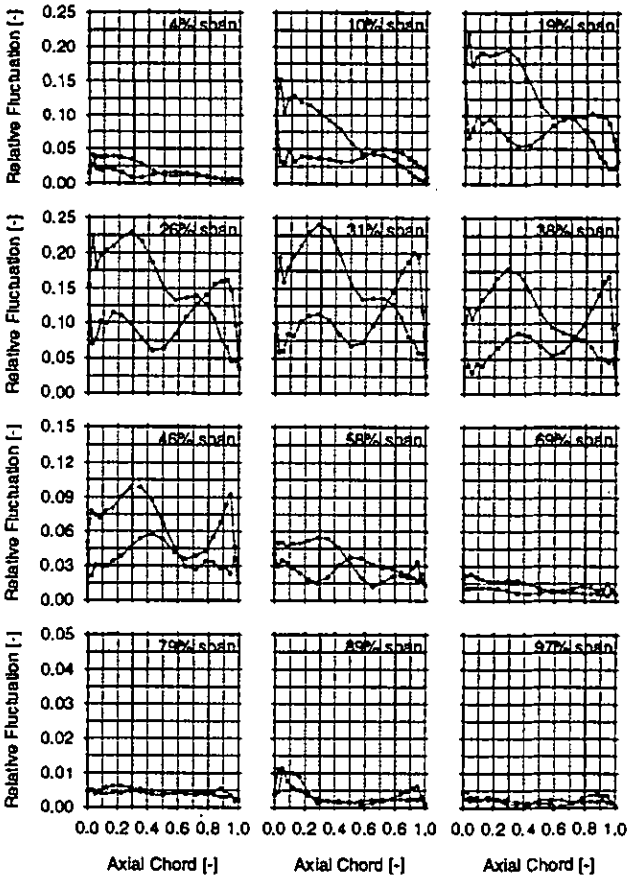

Figure 6: Relative temporal fluctuations of the unsteady rotor blade pressure distributions (circles: suction side, squares: pressure side)

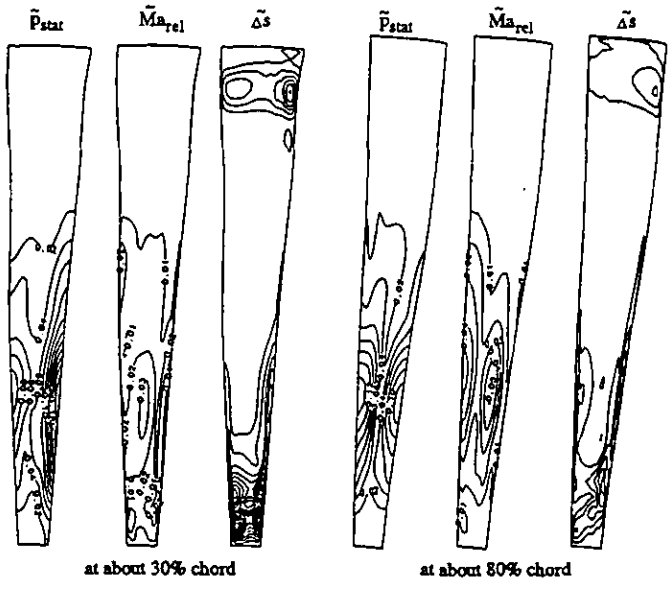

Figure 7: Lines of constant fluctuations of static pressure, relative Mach number and entropy in blade to blade passage of rotor

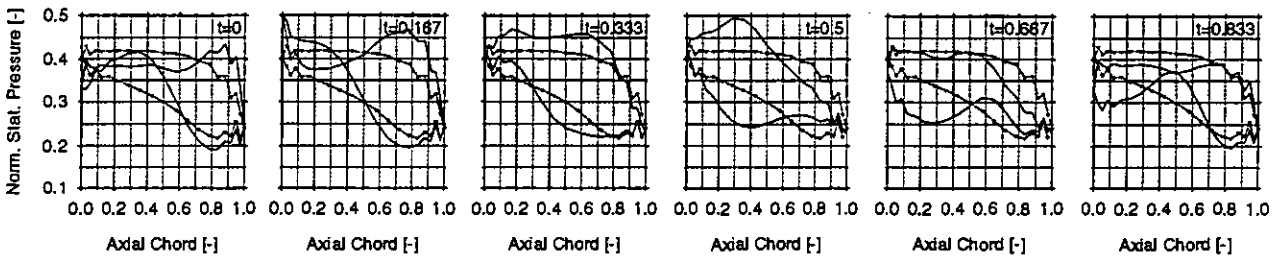

Figure 8: Instantaneous rotor blade pressure distributions (solid lines) and time-averaged values (symbols) at 31 % span

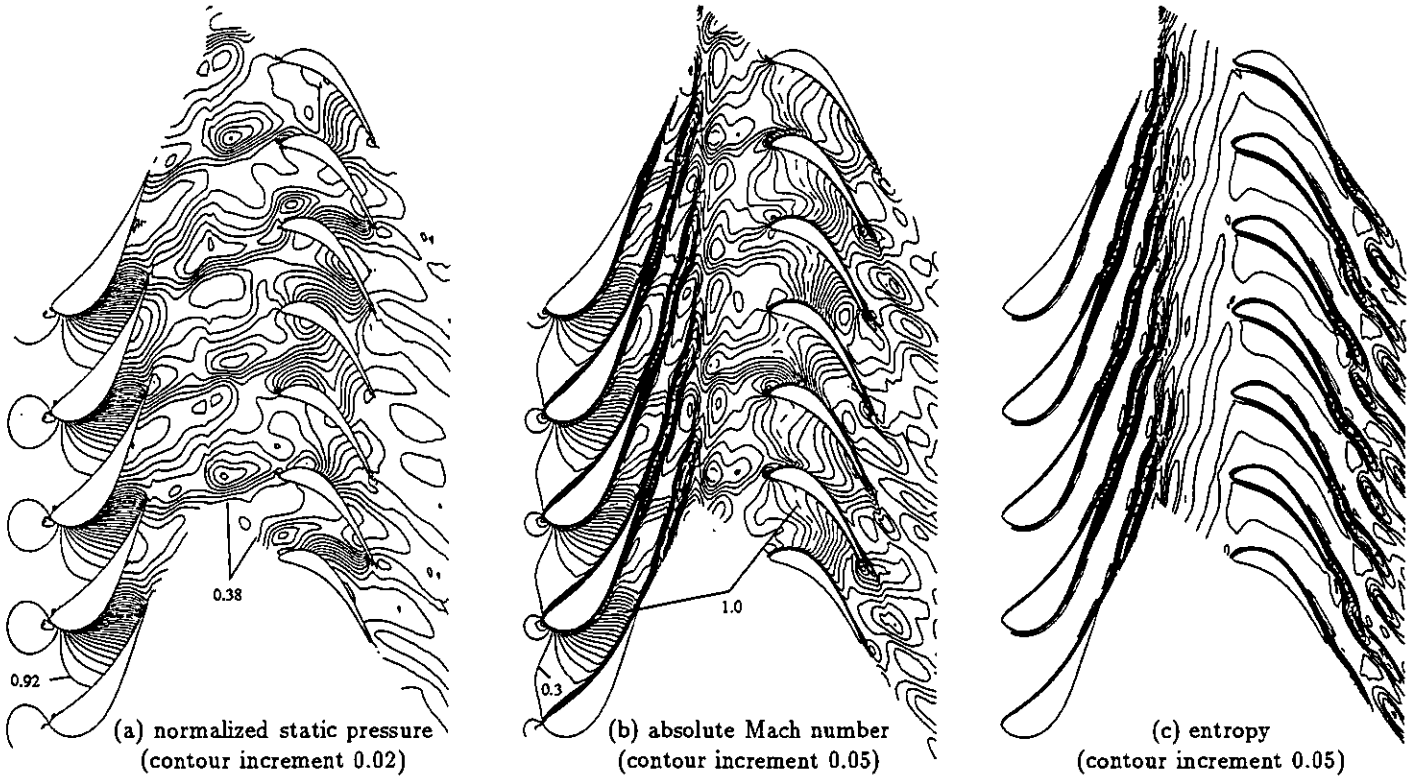

(a) normalized static pressure (contour increment 0.02)

(b) absolute Mach number (contour increment 0.05)

(c) entropy (contour increment 0.05)

Figure 9: Contour lines at 31 % span at time t=0

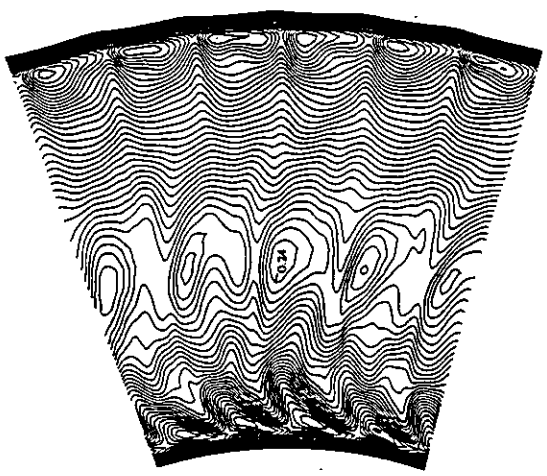

Figure 10: Relative Mach number contours (increment 0.02) at about 75 % of axial gap between stator and rotor at time t=0

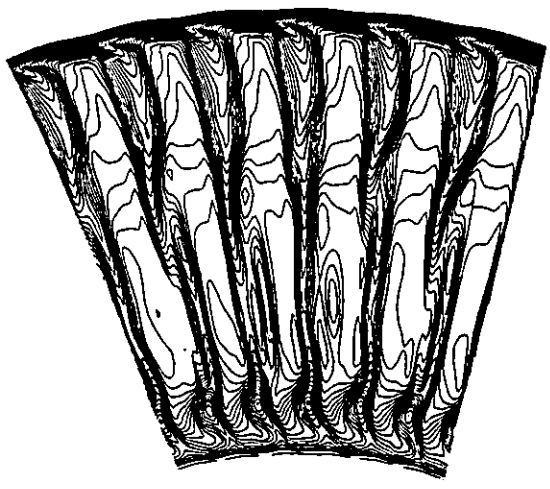

Figure 11: Instantaneous entropy contours near the outlet boundary of the rotor domain at time t=0